Journal of Thermal Analysis and Calorimetry, Vol. 56 (1999) 151–156

A STUDY ON THE THERMAL BEHAVIOUR OF SOLDER GLASS

Jinn-Shing Lee[1,2,3], *Chung-King Hsu*[1], *Li-Kuo Lin*[3,4], *Chih-Long Chang*[2], *Shich Borjinn*[2] *and Chin-Wang Huang*[2]

[1]Department of Material and Mineral Resources Engineering, National Taipei University of Technology, Taipei, Taiwan
[2]Department of Chemistry, Chung Yuan Christian University, Chungli, Taiwan
[3]Chung Shan Institute of Science and Technology, P.O. Box 90008-15-9, Lungtan, Taiwan
[4]Department of Chemical Engineering, National Central University, Chungli, Taiwan, R.O.C.

Abstract

Vitreous solder glasses, such as Mansol #40 and FEG-2002, are commercialized solder glasses, which are compression sealing glasses that can be used to solder materials with expansions between $55–68 \cdot 10^{-7}°C^{-1}$, such as Al_2O_3.

In order to understand and tailor the thermal behaviour of solder glasses, cylindrical-like glasses were first carefully ground with a stainless steel mortar and pestle. Initially, no exothermic or endothermic data were obtained from the DTA/DSC curves except those relating to melting. However, exothermic peaks appeared after the glass samples were re-melted. In this work, kinetic parameters such as the activation energy, and the morphology of the devitrification mechanisms for two kinds of solder glasses were also investigated, using non-isothermal DTA techniques. The activation energies ranged from 220 to 235 kJ mol^{-1} and the devitrification mechanism parameters were close to 1. This indicates that the devitrification mechanisms of the two kinds of solder glasses involve surface nuclei.

Keywords: activation energy, devitrification mechanism, FEG-2002, Mansol #40, solder glasses, thermal properties

Introduction

In order to meet the requirements for pyrotechnic devices such as initiators, detonators, etc., which must function reliably at high pressures after long storage times, many researchers have initiated research programs to develop better explosive device headers. Such headers usually use a glass or ceramic insulator to isolate the electrical feed, often through Kovar or copper alloy, from a stainless steel case. Glass ceramic-to-metal seals offer the greatest probability of meeting the consolidated header requirements. Most commercial headers with glass-to-metal seals are fabricated by using preforms of pressed and sintered glass powder; however, most glass-to-metal seals are weak. Glass-ceramics can be molded like glass and bonded directly to oxidized metal surfaces, but they are stronger, more refractory, and have higher thermal conductivities than glasses. Another advantage of glass-ceramics is

1418–2874/99/ $ 5.00

Akadémiai Kiadó, Budapest
Kluwer Academic Publishers, Dordrecht

that they can be made with a wide range of thermal expansion coefficient (0~$230 \cdot 10^{-7}$ °C^{-1}). Therefore, they permit great flexibility in seal design, and can be economically incorporated into the header design. In this work, two commercial solder glasses are introduced into the ceramic-to-metal sealing and the assembly parts for sealing, arranged as in Fig. 1. In order to understand the physical properties of these solder glasses, the thermal behaviour, linear thermal expansion coefficients and rates of helium leakage of hermetic seals have been investigated.

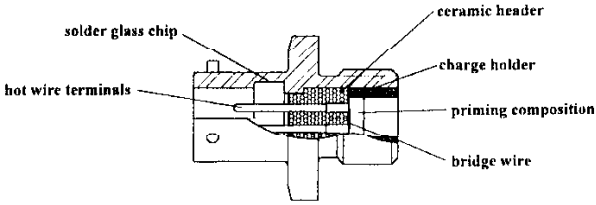

Fig. 1 Cross-section of pressure cartridge

Experimental

Two solder glass chips were supplied by Corning Corporation and Ferro Corporation. The compositions of the glasses were examined by using SPARK, XRF, ICP, and ignition loss methods, and are listed in Table 1. The sample powders were prepared by very careful crushing, using a stainless steel pestle and mortar, and then sieved in order to obtain fine particles (pass 325 mesh). DTA curves of approximately 30 mg of fine glass powders were recorded at different heating rates (2 to 20°C min^{-1}), under static air atmosphere.

Table 1 Compositions of solder glasses

Glasses	SiO_2	Al_2O_3	Na_2O	K_2O	BaO	B_2O_3	MgO	ZnO	PbO
	Composition/mass%								
Mansol #40	56.2	3.21	10.24	9.0	10.43	0.62			
FEG-2002	12.8	6.03			0.33	2.7	2.17	1.84	67.9

A Rigaku-Denki thermoanalyzer (model 8121) was used, with powdered α-Al_2O_3 as reference material. Heat treatment procedures were determined via DTA curves. Both sealing parts and glass chips were placed into the furnace and heat treatment was applied. Samples after heat treatment were subjected to hermetic testing, using an Ultratest (model UL 100 plus) helium detector (Leybold AG, Germany), and the crystallized phases of the resultant glasses were examined by powder X-ray diffraction (Rigaku-Denki).

Results and discussion

Figure 2 shows the DTA curves of the glass powders. Initially no exothermic or endothermic peaks were observed, except those relating to melting (Fig. 2, curves (1)–(4)). However, exothermic peaks appeared after the glass powder samples were re-melted (Fig. 2, curves (5) and (6)). Such a phenomenon may be due to the binder effect; after re-melting of the glass powder samples, the long-distance glass network was reconstructed.

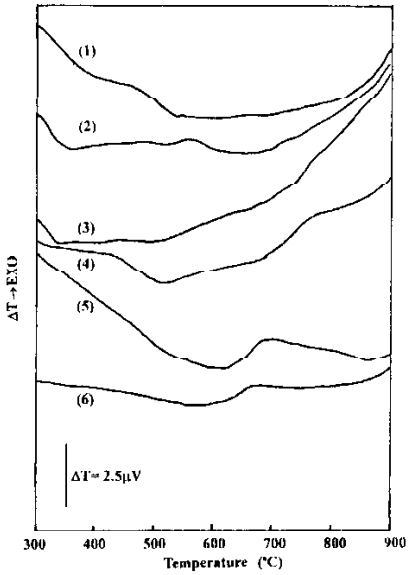

Fig. 2 DTA curves of solder glass powders under static air atmosphere at a heating rate of 10°C min^{-1}; 1 – Mansol #40 (≤ 44 μm); 2 – FEG-2002 (≤ 44 μm); 3 – Mansol #40(297–590 μm); 4 – FEG-2002(297–590 μm); 5 – Mansol #40(re-melted); 6 – FEG-2002 (re-melted)

When a glass is heated at a constant rate, crystal nuclei are formed at temperatures higher than the glass transition temperature and increase in size at higher crystallization temperatures, without any increase in number [1]. Differential scanning calorimetry (DSC) and differential thermal analysis (DTA) were used to observe the exothermic crystallization of the various species on re-heating of the glass powders. A variable heating rate method was used to determine the activation energies of crystallization. Rates of 2 to 20°C min^{-1} were used in the DTA measurements. The kinetic model [2] used is given by Eq. (1):

$$-\ln(1-\alpha) = \frac{AN}{h^m} \exp\frac{-mE_G}{RT} \quad (1)$$

where α is the volume fraction crystallized at temperature T, h is the DTA heating rate, A is a constant, and the parameter m depends on the mechanism and morphology of crystal growth.

For growth controlled by reaction at the glass-crystal interface, m ranges in value from 1 (for one-dimensional growth or growth from surface nuclei) to 3 (for three-dimensional growth). If we take into account [3] the fact that at the peak temperature (T_m) the degree of crystallization reaches the same specific value, independently of the heating rate, the following equation can be derived:

$$\ln h = -\frac{E_{G1}}{RT_m} + \text{const.} \tag{2}$$

$$\ln\left(\frac{h}{T_p^2}\right) = -\frac{E_{G2}}{RT_m} + \text{const.} \tag{3}$$

Moreover, since the deflection from the baseline, ΔT, is proportional to the instantaneous reaction rate [4], and since the change in temperature in the initial part of the DTA crystallization peak has a much larger effect than α on the ΔT deflection, the following equation can be obtained:

$$\ln \Delta T = -\frac{mE_G}{RT} + \text{const.} \tag{4}$$

Figure 3 shows composite plots of the DTA curves of the two solder glasses at heating rates of 2 to 20°C min^{-1}. For plots of $\ln\Delta T$ *vs.* $1/T$, and $\ln h$ *vs.* $1/T_m$, straight lines were obtained, and the values of the kinetic parameter E_G and m were calcu-

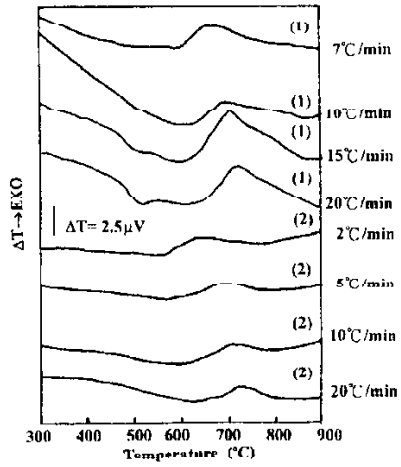

Fig. 3 DTA curves of solder glass powder under static air atmosphere at heating rates of 2–20°C min^{-1}; 1 – Mansol #40 (≤44 μm); 2 – FEG-2002 (≤44 μm)

lated from the slopes of these lines; the results are reported in Table 2. The values of m suggest that only surface crystallization takes place in the two re-melted glasses. These results confirm that, for the glass compositions studied, devitrification starts mainly from surface nuclei. The activation energies calculated from the slopes of linear least-squares fits to the data lay in the range 220–235 kJ mol^{-1} close to those reported by Lee *et al.* [5].

Table 2 Activation energies and parameter m for crystallization, evaluated by non-isothermal DTA techniques

Glasses	Range of T_m/°C	E_{G1}/ kcal mol^{-1}	E_{G2}/ kcal mol^{-1}	mE_G/ kcal mol^{-1}	$-r_{a1}$	$-r_{a2}$	$-r_{a3}$	$E_{G,avg}$/ kcal mol^{-1}	m
Mansol #40	672~706	56.1	52.4	56.3	0.981	0.973	0.983	54.3	1.04
FEG-2002	627~689	57.5	54.6	50.7	0.974	0.983	0.954	56.1	0.9

$-r_a$ – correlation coefficient for linear regression analysis of the Kissinger plot
E_{G1} – activation energy calculated by plotting $\ln h$ *vs.* $(1/T_p)\cdot 1000$
E_{G2} – activation energy calculated by plotting $\ln(h/T_p^2)$ *vs.* $(1/T_p)\cdot 1000$
mE_G – slope calculated by plotting $\ln\Delta T$ *vs.* $(1/T)\cdot 1000$

Figure 4 presents the XRD patterns of the resultant specimens. It is found that sodium barium silicate and lead aluminium silicate are formed as new crystalline phases on heat treatment. This will enhance the strength of the sealing parts, because glass-ceramics were found in solder glass matrices.

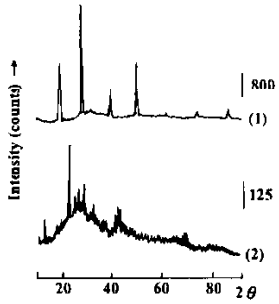

Fig. 4 Powder X-ray diffraction patterns (CuK_α) for solder glasses: 1 – FEG-2002 after heat treatment procedure, 2 – Mansol #40 after heat treatment procedure

The rates of helium leakage of the sealing parts ranged from $1\cdot10^{-5}$ to $1\cdot10^{-7}$ atm cm^3 s^{-1}. The linear thermal expansion coefficients of the two solder glasses proved to be $61.5\cdot10^{-7}$ °C^{-1} (25~300°C) for FEG-2002 and $71.0\cdot10^{-7}$ °C (25~300°C) for Mansol #40, which are sealing glasses that can be used to solder material with expansions between 55 and $68\cdot10^{-7}$ °C^{-1}, such as Al_2O_3.

Conclusions

Although much additional experimentation is necessary, we have confirmed that the combined efforts of our research, engineering and design of sealing parts will provide a solution compatible with our consolidated requirements. It can be concluded from the experimental results that the crystallization of Mansol #40 and FEG-2002 solder glasses is controlled by a surface crystallization mechanism, with activation energies of crystallization ranging from 220 to 235 kJ mol^{-1}.

References

1 K. Matusita and S. Sakks, Phys. Chem. Glasses, 20 (1979) 81.
2 F. Branda, A. Marotta and A. Buri, Thermochim. Acta, 128 (1988) 39.
3 T. Ozawa, Polymer, 12 (1971) 150.
4 A. Marotta, A. Buri and P. Pernice, Phys. Chem. Glasses, 21 (1980) 94.
5 J.-S. Lee, J. C. Perng and C. W. Huang, Thermochim. Acta, 162 (1990) 367.